Shahrood University of Technology
Iranian Society of Mining Engineering (IRSME)
Journal of Mining and Environment (JME)
journal homepage: www.jme.shahroodut.ac.ir
THOMSON REUTERS
Published online: 18 October 2019.
DOI: 10.22044/jme.2019.7489.1614

Fractal-wavelet-fusion-based re-ranking of joint roughness coefficients

M. Lotfi and B. Tokhmechi*

Faculty of Mining, Petroleum & Geophysics Engineering, Shahrood University of Technology, Shahrood, Iran

Received 24 October 2018; received in revised form 19 April 2019; accepted 1 June 2019

Keywords

Asperity

Dimension

Decision-Making

Data Fusion

Uncertainty

Abstract

Nowadays, Barton's Joint Roughness Coefficients (JRC) are widely used as the index for roughness and as a challenging fracture property. When JRC ranking is the goal, deriving JRC from different fractal/wavelet procedures can be conflicting. Complexity increases when various rankings outcome from different calculation methods. Therefore, using Barton's JRC, we cannot make a decision based on the proven mathematical theories because each method has a different rank. Ideally, these rankings must be equal but, in practice, they are different for each method. To solve this problem and to achieve a robust and valid ranking for JRC, Condorcetand Borda count methods have been used. These methods have been proposed as fusion approaches. Re-ranking of JRC using different methods integrated with Condorcet showed confusion in ranking of the JRC4, JRC5, and JRC6 profiles. This ambiguity is equal to equalizing decision conditions about all the three at the examination of the winners, losers, and draws in pairwise matrices. Therefore, Borda Count was applied and resulted in robust rankings. In fact, a new approach for a roughness measurement is presented. A new JRC ranking called JRCN is introduced. This new ranking shows a lower sum of squared errors (0.00390) in comparison with the original JRC ranking method (0.00410) and ranked $JRCN_1$ to $JRCN_{10}$. Thus it is proposed to consider JRCN as a new and improved version of JRC rankings.

1. Introduction

Roughness (asperity) is a challenging fracture property. Generally, roughness is defined as any deviation of the examined surface compared to the situation where the surface is completely flat [1]. Roughness of a fracture differs in various directions because of the tectonic and tension regimes. This level of dependence increases uncertainty. Also the expressed values stay away from the non-uniqueness amounts. Inasmuch as for measuring roughness in the 2D space, sufficient high-quality data with suitable rate is required, and it is not easy to do calculations on such a space; a criterion such as the well-known Joint Roughness Coefficient (JRC) exemplar profiles is required. Considering this approach, the results can be considered as the most widely used observational method for investigating the effect of roughness of fracture surface. Since the introduction of this concept [2, 3], the procedure was considered and modified by scientific communities. The researchers presented their reports on how roughness might be measured [4-9].

The wavelet, variogram analysis, roughness-length method (root mean square), as well as the fractal- based methods containing power spectral density (PSD), height-length, compass-walking, and divider method have been nominated as the common methods used for roughness measuring. Because of the difficulty in measuring fractal dimension, numbers of empirical relations between JRC values and roughness parameters with different definitions have been applied [9]. Similarity-based methods [10-16] and Hausdorff-based method [17-19] were also utilized for measuring the roughness.

Corresponding author: tokhmechi@ut.ac.ir (B. Tokhmechi).

In wavelet-based methods [20], rough profiles were considered as a signal, and were analyzed by the signal processing methods. Accordingly, Lee *et al*. (1998) determined the roughness and morphological characteristics of the surface with principles based on the wavelet transform equations [21]. In a similar study, Josso *et al*. (2000) used the frequency normalized wavelet transform (FNWT) strategy for surface roughness analysis and characterization [22- 24]. With such an approach, Asadi *et al*. (2009) analyzed the JRC exemplar profiles [25]. In the same year, Grzesik and Brol (2009) characterized the surface roughness of different workpiece materials using the fractal-based methods and wavelet transform [26]. Morala-Argüello *et al*. (2012) used the Haar mother wavelet to analyze the synthetic rough surfaces in four different classes [27]. Also Zou *et al*. (2015) impacted surface roughness on the flow of fluid using the finite volume method (FVM) and resolving Navier-Stokes equations relative to non-linear fluid flow in a single fracture [28].

The fractal-based methods used for studying, characterization, and quantifying the roughness of surfaces have been used extensively [29-44]. The value of power spectral density (PSD) can be calculated by fast Fourier transform (FFT) in one dimension and complex function in two dimensions [45- 47]. Additionally, the fractal dimension can be obtained by plotting the log-log diagram of energy versus the wave number [48, 49]. Jacobs *et al*. (2017) determined the quantitative characteristics of the topographic surface using the PSD method [50]. In the same year, Jain and Pitchumani (2017) analyzed the fractal model of rough surface to check the surface wettability [51]. In this regard, Mitra *et al*. (2017) studied the roughness for characteristic underwater micro-patterned surfaces based on the fractal model (Weierstrass−Mandelbrot function) [52]. Jain (2017) determined the fractal parameters using the power spectrum of the surface [53]. The variogram analysis method is a specific technique in spatial analysis [54, 55]. In this method, the fractal distribution is obtained through a variogram model and the calculation of the graph gradient for the relative distance of the pair of samples versus the variogram value in a log-log scale [56]. Perfect (2005) defined the drainage probability as the ratio of the volume of pore spaces to the total space using the fractal model [57]. Rasouli and Tokhmechi (2010) simulated reservoirs and provided an estimate of porosity using the geostatistical models based on fractal geometry [58]. Ojha *et al*. (2017) presented an estimation of the remaining saturation and relative permeability for organic-rich shale samples with a dual approach to the previous studies using the fractal-based method. They also intercepted the diameter of the pore size in their calculations [59]. Suleimanov *et al*. (2017) studied the effect of fractal dimension on flooding operation based on the analysis of the profile of oil well production [60]. In the roughness-length method, introduced by Malinverno (1990), the length of the rough profile was calculated based on the residual value of the root mean square (RMS) of a linear model. The fractal dimension was also obtained by plotting RMS versus window length in a log-log scale and calculating the gradient of the graph [61]. Rahman *et al*. (2004) derived roughness characteristics of rock mass discontinuities from the laser scanning data [62]. Also Arizabalo *et al*. (2004) utilized the roughness-length method, variogram analysis, and wavelet to analyze the wire-line logs in a naturally fractured limestone reservoir in the Gulf of Mexico [63]. In the height-length method, the fractal dimension to the desirable profile is achieved by considering a base line on the roughness profile and calculating the average height and average base length relative to baseline [64]. The relationship provided by Xie and Pariseau (1994) was later corrected by Askari and Ahmadi (2007), while it confirmed that the estimations were partly biased [65]. In the compass-walking method, roughness profile length is surveyed by considering a variable size of the divider. This process is performed by changing the length of the divider after completing each survey and repeating from the initial point similarly. Finally, fractal dimension will be obtained from the division of the changes of product of length of divider in repeated times relative to the lengths of divider in a log-log scale minus one [66]. Bae *et al*. (2011) added the remaining amount to this relation as an upgrade and calculated the fractal dimension of profiles [67]. Afterward, Li and Huang (2015) suggested a similar approach to measure the change of iterative calculation number relative to the length of divider in the log-log scale. These results were equivalent with fractal dimension (with a negative sign). Also they analyzed JRC using the height-length method [64], and the compass-walking (divider) method [66-68].

In this work, roughness of profiles was calculated using the fractal and wavelet methods. The results obtained were fused using Condorcet and Borda

Count. As the result of this procedure, a new robust ranking for JRC profiles was introduced.

2. Methodology

In the first step and before performing any analysis, the roughness profiles were digitized (Figure 1). The flowchart of the approach presented in this work is shown in Figure 2. Two utilized procedures for roughness calculation will be introduced, and also Condorcet and Borda Count, which are data fusion methods, will be explained.

2.1. Digitizing JRC profiles

The JRC profiles were digitized with a lag distance of 0.02 mm. Practically, each profile was considered as a signal, and the amount of "Y" axis for any "X" was measured (Figure 1). More than 5200 points were achieved for each profile, and the number of data was found to be 54710. This data was considered as the digitized JRC profile (Figure 1).

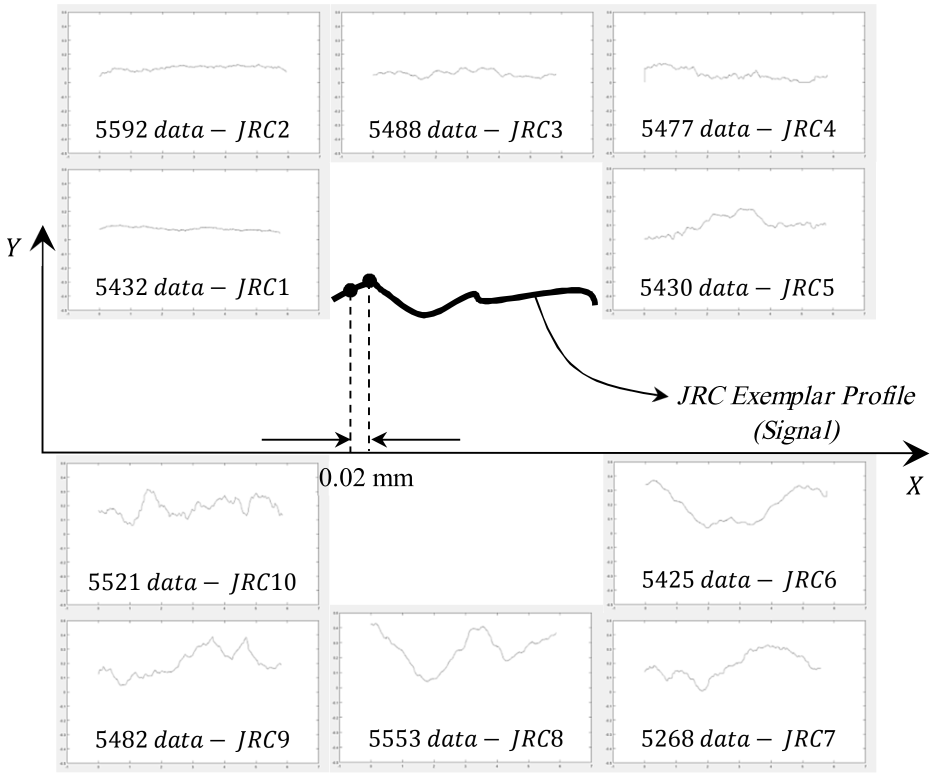

Figure 1. The process of digitizing JRC profiles. (In order to reveal the roughness changes, the profiles were rescaled in two axes (squeezed in the x-axis and stretched in the y-axis) but the calculations were done in the original scale.)

2.2. Fractal-based roughness calculation

In order to perform the fractal-based method, the fractal dimensions of the digitized JRC profiles (Figure 3) were calculated. Supposing the number of repeating of the survey is N (Figure 3), the fractal dimension of the desired profile can be obtained by plotting Nr versus r in a log-log scale; r is the length of divider (Equation 1-first method) [66].

$$D = 1 - \frac{\Delta \log(Nr)}{\Delta \log(r)} \quad (1)$$

In the second method [67], the calculations and measurements were done by adding the remaining value to the other parameters mentioned in the first method. In fact, the fractal dimension depends on the parameters N, r, and f; N is the number of steps for any survey (Figure 4) and r is the length of divider, which is constant for any step. The size of r increases by going to higher steps.

Nr is a part of the desired profile with length of divider (r). Considering f as the remaining length of profile (Figure 5), the length of profile is equivalent to $Nr + f$. Knowing these parameters, the fractal dimension of rough profile is as follows [67]:

$$-D = \frac{\Delta \log\left[N + \frac{f}{r}\right]}{\Delta \log r} \quad (2)$$

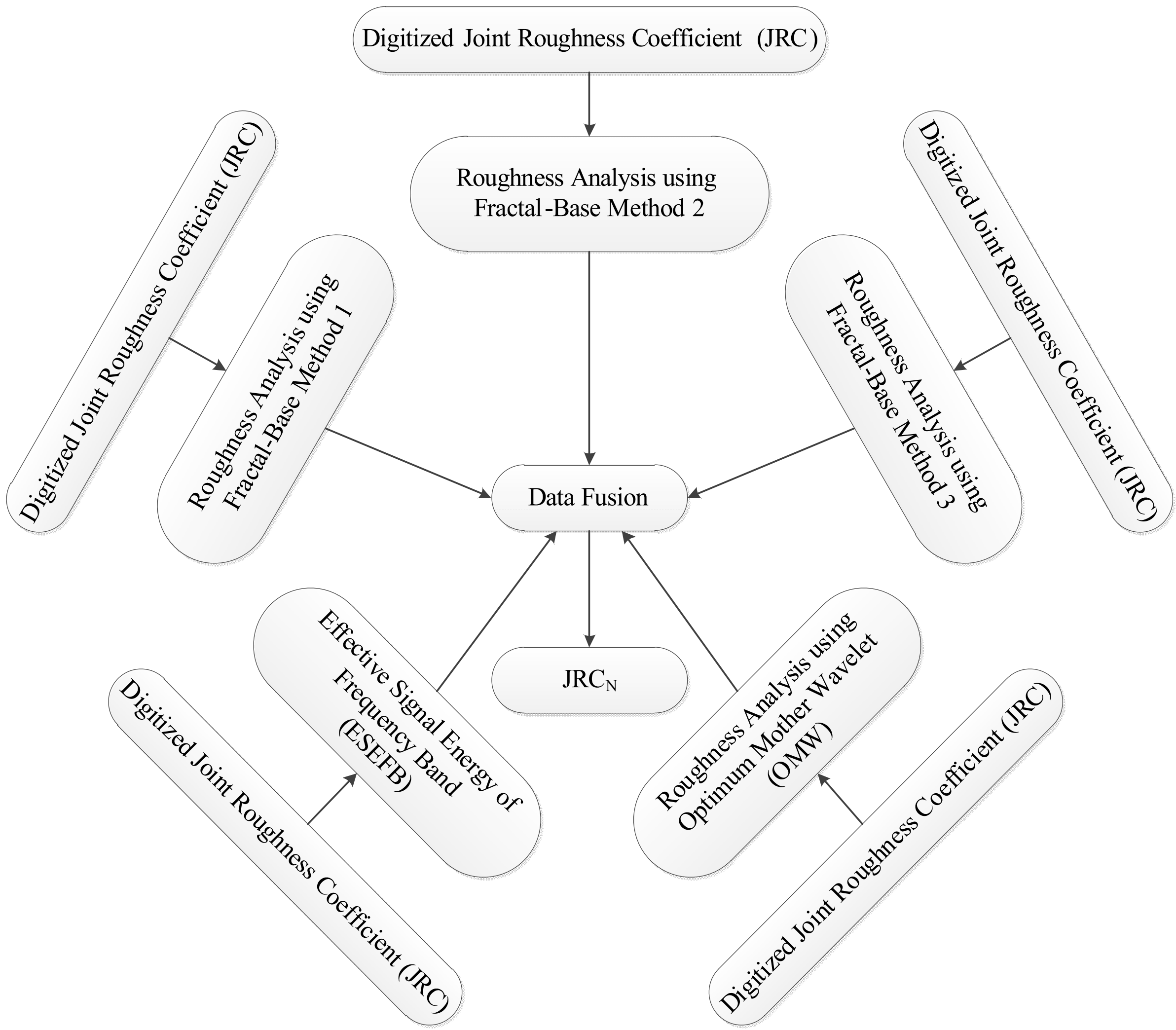

Figure 2. Flowchart of study.

Figure 3. Schematic representation of survey by applying method 1 ($N = 4$).

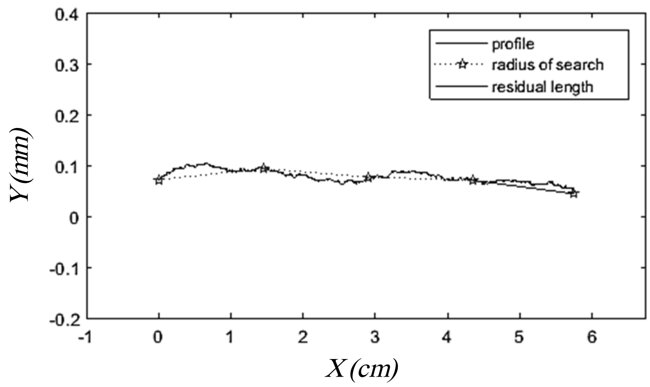

Figure 4. Surveying JRC_1 exemplar profile by applying method 2 ($N = 4$).

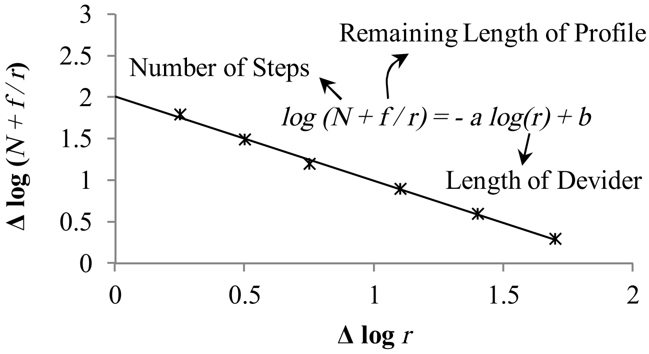

Figure 5. Calculation of fractal dimension using method 2.

In the third method, the fractal dimension is obtained by calculating the gradient of graph of N (step number) versus r (length of divider) [56]:

$$-D = \frac{\Delta \log N}{\Delta \log r} \tag{3}$$

2.3. Wavelet-based roughness calculation

In this method (Figure 6), continuous wavelet transform (CWT) was applied for analyzing the roughness of profiles (Equation 4). It was supposed that similarity occurred between the rough profile and signal $x(0)$. Fourier transform ($\hat{\Psi}(f)$) of the wavelet function ($\Psi(f)$) could be calculated using Equations 5 and 6 [20]. Semi-roughness could be calculated using Equation 7.

$$CWT_{x(u)}(\lambda,t) = \langle x, \psi_{\lambda,u} \rangle = \int_{-\infty}^{\infty} \psi_{\lambda,t}(u) x(u) du \tag{4}$$

$$\int_{-\infty}^{\infty} x^2(t) dt < \infty \tag{5}$$

$$C_\psi = \int_0^\infty \frac{\left|\hat{\psi}(f)\right|^2}{f} df, \left(0 < C_\psi < \infty\right) \tag{6}$$

$$x(t) = \frac{1}{C_\psi} \int_0^\infty \left[\int_{-\infty}^{\infty} \langle x, \psi_{\lambda,u} \rangle \psi_{\lambda,u}(t) du \right] \frac{d\lambda}{\lambda^2} \tag{7}$$

where λ is the scale parameter (positive), t is the transmission in a limited range, f is the frequency parameter, and u is the time.

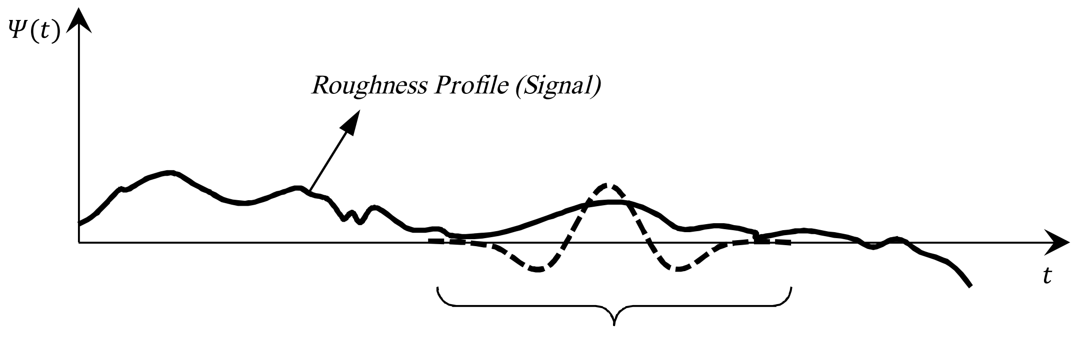

Figure 6. Schematic representation of accommodation between roughness profile (signal) and local wavelet in the wavelet-based process.

2.4. Condorcet data fusion

The Condorcet data fusion method is a decision-making method, where only one winner will be introduced. The winner is an option in which the Condorcet criterion is observed [69, 70]. In this method, the results obtained might be compared together. For this purpose, a pairwise matrix should be created. Afterwards, the winner, loser, and equal results should be counted; this is the criterion for decision-making [71, 72]. For example, consider $\boldsymbol{PWM}$ as a pairwise matrix between three features using five methods (M_1 to M_5):

$$
\begin{aligned}
M_1 &= \{F_1, F_2, F_3\} = \{F_1 > F_2 > F_3\} \\
M_2 &= \{F_1, F_3, F_2\} = \{F_1 > F_3 > F_2\} \\
M_3 &= \{F_1, F_2 and F_3\} = \{F_1 > F_2 = F_3\} \\
M_4 &= \{F_2, F_1\} = \{F_2 > F_1\} \\
M_5 &= \{F_3, F_1\} = \{F_3 > F_1\}
\end{aligned} \tag{8}
$$

$$
PWM = \begin{array}{c} \\ F_1 \\ F_2 \\ F_3 \end{array}
\begin{array}{c} \begin{array}{ccc} F_1 & F_2 & F_3 \end{array} \\ \begin{bmatrix} - & f_{12} & f_{13} \\ f_{21} & - & f_{23} \\ f_{31} & f_{32} & - \end{bmatrix} \end{array}
= \begin{array}{c} \\ F_1 \\ F_2 \\ F_3 \end{array}
\begin{array}{c} \begin{array}{ccc} F_1 & F_2 & F_3 \end{array} \\ \begin{bmatrix} - & \underbrace{4,1,0}_{f_{12}} & 4,1,0 \\ 1,4,0 & - & 2,2,1 \\ 1,4,0 & 2,2,1 & - \end{bmatrix} \end{array} \tag{9}
$$

Based on the example, f_{12} is equal to "4,1,0" in a double confrontation between feature i and feature j (here, feature 1 *vs.* feature 2). In the stated amount, "4", "1", and "0" are the numbers of wining, losing, and equality of F_1 (feature 1) compared with F_2 (feature 2), respectively. Therefore, all numbers for wining, losing, and equality might be counted.

2.5. Borda count data fusion

In this method, the data must be rated based on the position in the first step. Thus the first feature takes the highest score. The scores of the next features are reduced by one unit, respectively [72, 73]. For example, the scores of features in $M_1 = \{F_1, F_2, F_3\}$ are 3, 2, and 1, respectively. Thus it can be written as "F_1^3", "F_2^2", and "F_3^1" (F_{Number}^{Score}). This scoring should be done for all methods. To calculate each score, the score points are counted in each position cumulatively. Since the Borda scoring method can cover the problem of equilibrium of Condorcet, this method can be used for ambiguity and uncertainty.

3. Results

In this part, fractal analysis of JRC, wavelet analysis of JRC, and decision-making based on data fusion including Condorcet method and Borda Count are explained.

3.1. Fractal analysis of JRC

Regardless of the method for calculation and measurement of rough profiles (JRC exemplar profiles), it is expected that with increase in the number of profiles, the corresponding dimension for any profile increases. This is shown in Figure 7 for each method.

The results obtained for all methods (Figure 7) show that there is no straightforward relation between the JRC ranking and the calculated roughness. To overcome this problem, the results obtained might be fused. Table 1 shows the fractal dimension before and after ranking of JRC and re-ranking of the profiles.

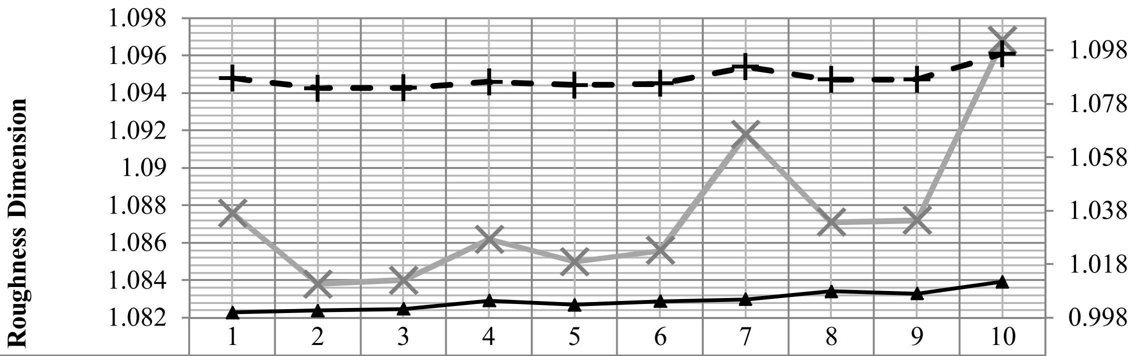

	1	2	3	4	5	6	7	8	9	10
Method 1	1.0876	1.0838	1.084	1.0862	1.085	1.0856	1.0918	1.0871	1.0872	1.0968
Method 2	1.0001	1.0008	1.0014	1.0045	1.0029	1.0043	1.005	1.008	1.0071	1.0116
Method 3	1.0876	1.0838	1.084	1.0862	1.085	1.0856	1.0918	1.0871	1.0872	1.0968

Profile No.

Figure 7. Results Obtained from calculation and measurement based on fractal geometry for each method.

Table 1. Rankings obtained using fractal-based methods.

Method number	Profile No. before ranking	Fractal dimension before ranking	Fractal dimension after ranking	Profile No. after ranking
1	1	1.0876	1.0838	2
	2	1.0838	1.0840	3
	3	1.0840	1.0850	5
	4	1.0862	1.0856	6
	5	1.0850	1.0862	4
	6	1.0856	1.0871	8
	7	1.0918	1.0872	9
	8	1.0871	1.0876	1
	9	1.0872	1.0918	7
	10	1.0968	1.0968	10
2	1	1.0001	1.0001	1
	2	1.0008	1.0008	2
	3	1.0014	1.0014	3
	4	1.0045	1.0029	6
	5	1.0029	1.0043	4
	6	1.0043	1.0045	5
	7	1.0050	1.0050	7
	8	1.0080	1.0071	9
	9	1.0071	1.0080	8
	10	1.0116	1.0116	10
3	1	1.0876	1.0838	2
	2	1.0838	1.0840	3
	3	1.0840	1.0850	5
	4	1.0862	1.0856	6
	5	1.0850	1.0862	4
	6	1.0856	1.0871	8
	7	1.0918	1.0872	9
	8	1.0871	1.0876	1
	9	1.0872	1.0918	7
	10	1.0968	1.0968	10

3.2. Wavelet analysis of JRC

Re-ranking of JRC profiles based on Effective Signal Energy of Frequency Band (ESEFB) of wavelet and Optimum Mother Wavelet (OMW) is presented in Tables 2 and 3.

Table 2. Re-ranking of JRC obtained using wavelet-based method (Effective Signal Energy of Frequency Band (ESEFB) approach).

Profile No. before ranking	Effective signal energy of frequency band (ESEFB) (%)	Obtained dimension from ESEFB	Obtained ranking dimension from ESEFB	Profile No. after ranking
1	99.84	1.0900	1.0900	1
2	99.52	1.0897	1.0897	2
3	96.59	1.0870	1.0896	7
4	97.58	1.0879	1.0880	(9 or 10)
5	90.16	1.0810	1.0880	(10 or 9)
6	89.12	1.0800	1.0879	4
7	99.46	1.0896	1.0870	3
8	95.79	1.0862	1.0862	8
9	97.71	1.0880	1.0810	5
10	97.71	1.0880	1.0800	6

Table 3. Re-ranking of JRC obtained using the wavelet-based method. Optimum Mother Wavelet (OMW) approach.

Profile No. before ranking	Optimum mother wavelet	Optimum mother wavelet energy (OMWE) (%)	Obtained dimension from OMWE	Obtained ranking dimension	Profile No. after ranking
1	rbio 3.3	99.84	1.0900	1.0900	1
2	rbio 3.3	99.78	1.0898	1.0899	7
3	rbio 3.1	96.60	1.0807	1.0898	2
4	rbio 3.3	97.78	1.0841	1.0875	6
5	rbio 3.3	97.56	1.0834	1.0874	8
6	rbio 3.7	98.96	1.0875	1.0853	9
7	rbio 3.1	99.83	1.0899	1.0841	4
8	rbio 3.3	98.94	1.0874	1.0834	5
9	rbio 3.3	98.22	1.0853	1.0807	3
10	rbio 3.1	96.37	1.0800	1.0800	10

4. Discussion

Different re-rankings of JRC obtained from the utilized methods are subjected to ambiguity and uncertainty. The Condorcet criterion means that when there are more than two options, the winner should overcome all of them [74]. Therefore, the number of winners, losers, and equals might be considered. To do this, the results obtained were fused with Condorcet (Figure 8), making a decision matrix (Figure 9) [20]. The decision matrix can be simplified. According to the decision matrix obtained from the Condorcet data fusion method, the profile numbers 4, 5, and 6 gained equal score (Figure 9).

For decision-making, Borda count was used [73], and the final score was gained.

Naturally, the positions of the equal options are the same. Thus scores of profiles 4, 5, and 6 are 27, 26, and 29, respectively. The results of this method were fused with the results obtained from Condorcet, and the final ranking was achieved (Figure 10).

$$Method_1 = \left\{JRC_2^{10}, JRC_3^{9}, JRC_5^{8}, JRC_6^{7}, JRC_4^{6}, JRC_8^{5}, JRC_9^{4}, JRC_1^{3}, JRC_7^{2}, JRC_{10}^{1}\right\}$$

$$Method_2 = \left\{JRC_1^{10}, JRC_2^{9}, JRC_3^{8}, JRC_6^{7}, JRC_4^{6}, JRC_5^{5}, JRC_7^{4}, JRC_9^{3}, JRC_8^{2}, JRC_{10}^{1}\right\}$$

$$Method_3 = \left\{JRC_2^{10}, JRC_3^{9}, JRC_5^{8}, JRC_6^{7}, JRC_4^{6}, JRC_8^{5}, JRC_9^{4}, JRC_1^{3}, JRC_7^{2}, JRC_{10}^{1}\right\}$$

$$Method_{DESEFB} = \left\{JRC_1^{10}, JRC_2^{9}, JRC_7^{8}, JRC_9^{7}, JRC_{10}^{7}, JRC_4^{5}, JRC_3^{4}, JRC_8^{3}, JRC_5^{2}, JRC_6^{1}\right\}$$

$$Method_{DOMWE} = \left\{JRC_1^{10}, JRC_7^{9}, JRC_2^{8}, JRC_6^{7}, JRC_8^{6}, JRC_9^{5}, JRC_4^{4}, JRC_5^{3}, JRC_3^{2}, JRC_{10}^{1}\right\}$$

	JRC_1	JRC_2	JRC_3	JRC_4	JRC_5	JRC_6	JRC_7	JRC_8	JRC_9	JRC_{10}
JRC_1	-	3,2,0	3,2,0	3,2,0	3,2,0	3,2,0	5,0,0	3,2,0	3,2,0	5,0,0
JRC_2	2,3,0	-	5,0,0	5,0,0	5,0,0	5,0,0	4,1,0	5,0,0	5,0,0	5,0,0
JRC_3	2,3,0	0,5,0	-	3,2,0	4,1,0	4,1,0	3,2,0	4,1,0	3,2,0	4,1,0
JRC_4	2,3,0	0,5,0	2,3,0	-	3,2,0	1,4,0	3,2,0	4,1,0	3,2,0	4,1,0
JRC_5	2,3,0	0,5,0	1,4,0	2,3,0	-	3,2,0	3,2,0	3,2,0	3,2,0	4,1,0
JRC_6	2,3,0	0,5,0	1,4,0	4,1,0	2,3,0	-	3,2,0	4,1,0	4,1,0	4,1,0
JRC_7	0,5,0	1,4,0	2,3,0	2,3,0	2,3,0	2,3,0	-	3,2,0	3,2,0	5,0,0
JRC_8	2,3,0	0,5,0	1,4,0	1,4,0	2,3,0	1,4,0	2,3,0	-	3,2,0	4,1,0
JRC_9	2,3,0	0,5,0	2,3,0	2,3,0	2,3,0	1,4,0	2,3,0	2,3,0	-	4,0,1
JRC_{10}	0,5,0	0,5,0	1,4,0	1,4,0	1,4,0	1,4,0	0,5,0	1,4,0	0,4,1	-

Figure 8. Pairwise matrix using Condorcet data fusion method for the results obtained for all methods.

	win	lost	draw
JRC1	9	0	0
JRC2	8	1	0
JRC3	7	2	0
JRC4	5	4	0
JRC5	5	4	0
JRC6	5	4	0
JRC7	3	6	0
JRC8	2	7	0
JRC9	1	7	1
JRC10	0	8	1

Figure 9. Decision matrix, applying the Condorcet method on pairwise matrix.

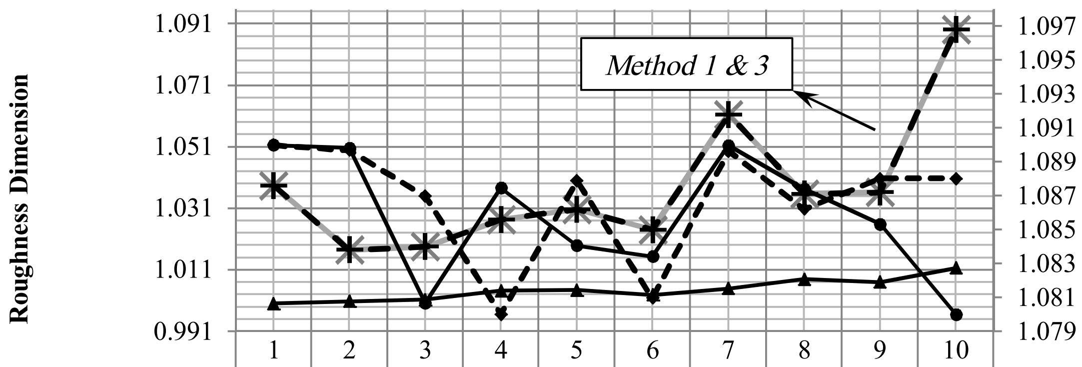

	1	2	3	4	5	6	7	8	9	10
JRCN (Method 2)	1.0001	1.0008	1.0014	1.0043	1.0045	1.0029	1.0050	1.0080	1.0071	1.0116
JRCN (Method 1)	1.0876	1.0838	1.084	1.0856	1.0862	1.085	1.0918	1.0871	1.0872	1.0968
JRCN (Method 3)	1.0876	1.0838	1.084	1.0856	1.0862	1.085	1.0918	1.0871	1.0872	1.0968
JRCN (DEFBSE)	1.0900	1.0897	1.0870	1.0800	1.0879	1.0810	1.0896	1.0862	1.0880	1.0880
JRCN (DOMWE)	1.0900	1.0898	1.0807	1.0875	1.0841	1.0834	1.0899	1.0874	1.0853	1.0800

Profile No.

Figure 10. Ranking JRC exemplar profiles after data fusion and turning it into the New JRC (JRC_N).

The statuses of the three profiles were compared with the original trend line (Figure 11) by calculating the error value in accordance with the Manhattan norm (Equation 10) [75].

$$\|p-q\|_1 = \sum_{i=1}^{n} |p_i - q_i| \quad (10)$$

The results that represent the final rankings are shown in Figure 12. The newly ranked profiles (JRC_N) can provide improved results compared to the original ranking (JRC). The results of Condorcet confirmed the original ranking despite an ambiguity in the profiles 4, 5, and 6. Borda Count was used to achieve a robust ranking. It should be mentioned that the sum of squared error (SSE) of the original JRC is equal to 0.00410 based on the Manhattan norm; while it is 0.00390 for the newly ranked. This shows a better trend for JRC_N. The suggested ranking is presented in Figure 12. In other words, if we want to judge about the roughness of custom profile by referring to JRC or decide on any other issue based on Barton's JRC [76], this judgment will be controversial; while it can be claimed that decision considering powerful methods based on proven theories (JRCN) is defensible and reliable. Another important point is to move away from differences in decision-making and convergence of expert opinions to each other. This is possible with the basis of SSE.

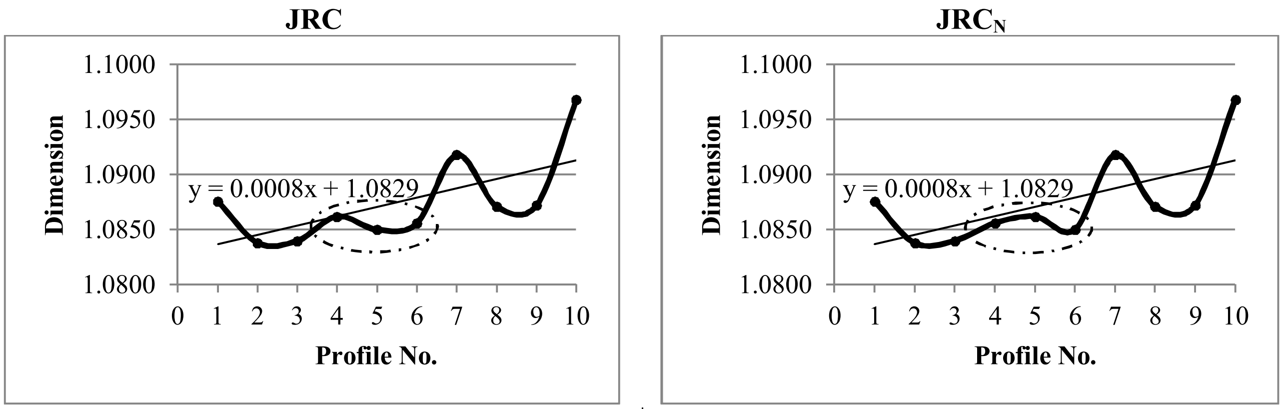

Method	error	Method	error
Manhattan norm	0.00410	*Manhattan norm*	0.00390

Figure 11. Calculation of error (SSE) using the Manhattan norm.

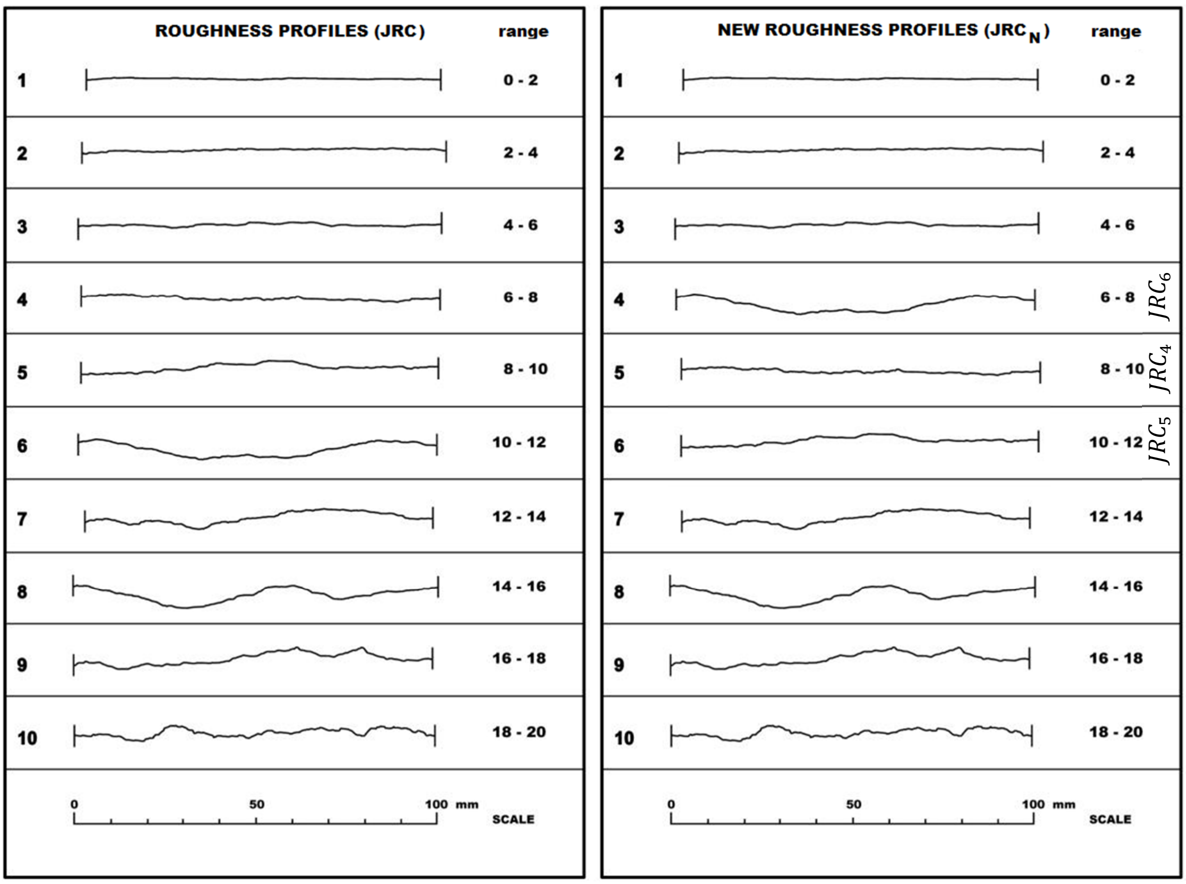

Figure 12. Roughness of exemplar profiles before (JRC in left) and after (JRC_N in right) re-ranking using the data fusion-fractal-wavelet-based approach.

5. Conclusions

The JRC profiles are widely utilized to rank the roughness of the fractures. Digitizing and analyzing of JRC profiles have confirmed that ranking of these profiles is challenging. In this work, a data fusion-based approach was utilized to achieve a robust ranking for the JRC profiles. In fact, calculation methods based on the definitive approach in assigning quantity dimension to roughness values can be a reliable indicator in validating JRC.

Different fractal/wavelet-based methods were used, and resulted in distinct semi-generalized ranking of JRC, showing the necessity of re-ranking of JRC profiles because each method provided a different response from the other methods about decision based on the Barton's JRC index. To achieve a more reliable ranking, the rankings obtained as the outcomes from each method were fused and integrated using the Condorcet and Borda Count methods. Condorcet showed ambiguity about ranking of the JRC4, JRC5, and JRC6 profiles. This ambiguity is the equality of the number of wins, losses, and draws in pairwise matrix for these example profiles. Thus the Borda Count position-based method was applied to assign proportional score to the achieved rankings. Based on the results obtained, addressed JRCN, profile 6 was moved to the fourth place, while the sequence of others remained stable. Consequently, the Manhattan-based SSE decreased from 0.00410 (original JRC) to 0.00390 (JRCN). Obviously, this result, after accurate measurements, suggests that the trend based on JRCN will be more rational. Also it can be concluded that the achieved ranking is, in fact, an extension of the Barton's pattern, which can be accepted as a new and more accurate and reliable applicable pattern.

References

[1]. Hudson, J.A. and Harrison, J.P. (1997). Engineering Rock Mechanics: An Introduction to the Principles. Elsevier Science Ltd.

[2]. Barton, N. (1973). Review of a new shear strength criterion for rock joints. Engineering Geology. 7: 287-332.

[3]. Barton, N. and Choubey, V. (1977). The shear strength of rock joints in theory and practice. Rock Mechanics and Engineering Geology. 10: 1-54.

[4]. Grasselli, G. and Tatone, B.S.A. (2010). A new 2D discontinuity roughness parameter and its correlation with JRC. International Journal of Rock Mechanics & Mining Sciences. 47: 1391-1400.

[5]. Ghazvinian, A. and Mohebi, M. (2012). Investigation and correcting factors offering for roughness corresponding to Barton Standard classes with quantitative fractal techniques. 4th Conference on Mining Engineering. University of Tehran. Iran, pp. 55-61 (in Persian).

[6]. Amanloo, F. and Hosseinitoudeshki, V. (2013). The effect of joint roughness coefficient (JRC) and joint compressive strength (JCS) on the displacement of tunnel. International Research Journal of Applied and Basic Sciences, Science Explorer Publications. 4 (8): 2216-2224.

[7]. Fathi, A., Moradian, Z., Rivard, P., Ballivy, G. and Boyd, A.J. (2016). Geometric effect of asperities on shear mechanism of rock joints. Rock Mech Rock Eng. 49 (3): 801-820.

[8]. Wang, C.H. and Guo, B. (2016). 2D and 3D Roughness Coefficient of Marble Joint Surface. EJGE, 21, Bund. 12: 4359-4368.

[9]. Yong, R., Ye, J., Liang, Q.F., Huang, M. and Du, S.G. (2018). Estimation of the joint roughness coefficient (JRC) of rock joints by vector similarity measures. Bull Eng Geol Environ. Springer. DOI 10.1007/s10064-016-0947-6.

[10]. Wu, D. and Mendel, J.M. (2008). A vector similarity measure for linguistic approximation: interval type-2 and type-1 fuzzy sets. Inform Sci. 178 (2): 381-402.

[11]. Ye, J. (2011). Cosine similarity measures for intuitionistic fuzzy sets and their applications. Math Comput Model 53 (1): 91-97.

[12]. Ye, J. (2012). Multicriteria decision-making method using the Dice similarity measure based on the reduct intuitionistic fuzzy sets of interval-valued intuitionistic fuzzy sets. Appl Math Model. 36 (9): 4466-4472.

[13]. Broumi, S. and Smarandache, F. (2013). Several similarity measures of neutrosophic sets. Neutrosophic Sets Syst 1 (1): 54-62.

[14]. Majumdar, P. and Samanta, S.K. (2014). On similarity and entropy of neutrosophic sets. J Intell Fuzzy Syst 26 (3): 1245-1252.

[15]. Ye, J. (2014). Vector similarity measures of hesitant fuzzy sets and their multiple attribute decision making. Econ Comput Econ Cybern Stud Res. 48 (4).

[16]. Ye, J. (2015). Improved cosine similarity measures of simplified neutrosophic sets for medical diagnoses. Artif Intell Med. 63: 171-179.

[17]. Orey, S. (1970). Gaussian sample functions and the Hausdorff dimension of level crossings. Probability Theory and Related Fields. (15) 3: 249-256.

[18]. Tatone, B.S.A. (2009). Quantitative Characterization of Natural Rock Discontinuity Roughness In-situ and in the Laboratory. MS Thesis. University of Toronto. 188 P.

[19]. Martišek, D. (2017). Joint Rock Coefficient Estimation Based on Hausdorff Dimension, Advances in Pure Mathematics. 7: 615-640.

[20]. Tokhmechi, B., Lotfi, M., Seifi, H. and Hosseini, M.S. (2016). Data Fusion, A New Approach for Decision Making in Geology, Mining and Petroleum Engineering, Amirkabir University of Technology

(Tehran Polytechnic) Press, Tehran, p. 808, ISBN: 978-964-463-656-1 (in Persian).

[21]. Lee, S.H., Zahouani, H., Carenti, R. and Mathia, T.G. (1998). Morphological characterization of engineered surfaces by wavelet transform. Int. J. Mach. Tools Manuf. (28): 581-589.

[22]. Josso, B. (2000). New wavelet-based space-frequency analysis methods applied to the characterisation of three-dimensional engineering surface textures. Ph.D. Thesis. Liverpool John Moores University.

[23]. Josso, B., Burton, D.R. and Lalor, M.J. (2001). Wavelet strategy for surface roughness analysis and characterization. Comput. Methods Appl. Mech. Eng. 191 (8-10): 829-842.

[24]. Josso, B,, Burton, D.R. and Lalor, M.J. (2002). Frequency normalized wavelet transform for surface roughness analysis and characterization. Wear. 252: 491-500.

[25]. Asadi, M.S., Rasouli,V. and Tokhmechi, B. (2009). Wavelet analysis of JRC exemplar profiles. Eurock 2009, Croatia: Balkema, pp. 215-220.

[26]. Grzesik, W. and Brol, S. (2009). Wavelet and fractal approach to surface roughness characterization after finish turning of different workpiece materials. Journal of Materials Processing Technology. 209 (5): 2522-2531.

[27]. Morala-Argüello, P., Barreiro, J. and Alegre, E. (2012). A evaluation of surface roughness classes by computer vision using wavelet transform in the frequency domain. Int. J. Adv. Manuf. Technol. 59 (1-4): 213-220.

[28]. Zou, L., Jing, L. and Cvetkovic, V. (2015). Roughness decomposition and nonlinear fluid flow in a single rock fracture. International Journal of Rock Mechanics & Mining Sciences. 75: 102-118.

[29]. Brown, S.R. (1987). A note on the description of surface roughness using fractal dimension. Geophys. Res. Lett. 14 (11): 1095-1098.

[30]. Pande, C.S., Richards, L.R. and Smith, S. (1987). Fractal characteristics of fractured surfaces. J. Met. Sci. Lett. 6: 295-297.

[31]. Dubuc, B., Quiniou, J.F., Roques-Carmes, C., Tricot, C. and Zucker, S.W. (1989). Evaluating the fractal dimension of profiles. Phys. Rev. A 39 (3): 1500-1512.

[32]. Miller, S.M., McWilliams, P.C. and Kerkering, J.C. (1990). Ambiguities in estimating fractal dimensions of rock fracture surfaces. Hustrulid, W., Johnson, G.A., Rock Mech. Contribution Challenges. Balkema, Rotterdam. pp. 471-478.

[33]. Dierking, W. (1999). Quantitative roughness characterization of geological surfaces and implications for radar signature analysis. IEEE Transactions on Geoscience and Remote Sensing. 37 (5).

[34]. Huang, S.L., Oelfke, S.M. and Speck, R.C. (1992). Applicability of fractal characterization and modeling to joint profiles. Int. J. Rock Mech. Min. Sci. Geomech. Abstr. 29 (2): 89-98.

[35]. Brown, S.R. (1995). Simple mathematical model of a rough fracture. J. Geophys. Res. 100: 5941-5952.

[36]. Schmittbuh, J., Vilotte, J.P. and Roux, S. (1995). Reliability of self-affine measurements. Phys. Rev. E 51 (1): 131-147.

[37]. Den Outer, A., Kasshoek, J.F. and Hack H.R.G.K. (1995). Difficulties with using continuous fractal theory for discontinuity surfaces. Int. J. Rock Mech. Min. Sci. Geomech. Abstr. 32 (1): 3-9.

[38]. Glover, P.W.J., Matsuki, K., Hikima, R. and Hayashi, K. (1998). Fluid flow in synthetic rough fractures and application to the hachimantai geothermal hot dry rock test site. J. Geophys. Res. 103 (B5): 9621-9635.

[39]. Develi, K. and Babadagli, T. (1998). Quantification of natural fracture surfaces using fractal geometry. Math. Geol. 30 (8): 971-998.

[40]. Glover, P.W.J., Matsuki, K., Hikima, R. and Hayashi, K. (1999). Characterizing rock fractures using synthetic fractal analogues. Geotherm. Sci. & Tech. 6: 83-112.

[41]. Babadagli, T. and Develi, K. (2001). On the application of methods used to calculate fractal dimension of fracture surfaces. Fractals 9 (1): 105-128.

[42]. Ogilvie, S.R., Isakov, E. and Glover, P.W.J. (2002). Advances in the characterization of rough fractures in reservoir rocks. First Break. 20 (4): 233-239.

[43]. Murata, S., Mitsuishi, H. and Saito, T. (2002). Characterization of fracture permeability by using a fractal model. SPE 77881. Proceedings of the Asia Pacific oil and Gas Conference and Exhibition. Melbourne, Australia. 8-10: 1-8.

[44]. Seno, T. (2003). Fractal asperities, invasion of barriers, and interplate earthquakes. Earth Planets Space. 55: 649-665.

[45]. Brigham, O.E. (1974). The fast fourier transform. Prentice-Hall, Inc. New Jersey. 133 P.

[46]. Saupe, D. (1988). Algorithms for random fractals, in: Saupe, D., Peitgen, H.O., eds., The science of fractal image: Springer-Verlag, New York. pp. 71-113.

[47]. Press, W.H., Teukolsky, S.A., Vetterling, W.T. and Flannery, B.P. (1992). Numerical recipes in C: The art of scientific computing. Cambridge University Press, USA. 504 P.

[48]. Berry, M.V. and Lewis, Z.V. (1980). On the Weierstrass-Mandelbrot fractal function. Proc. Roy. Soc. London. Ser. A. 370: 459-484.

[49]. Brown, S.R. and Scholz, C.H. (1985). Broad bandwidth study of the topography of natural rock surfaces. Jour. Geophys. Res. 90 (14): 12575-12582.

[50]. Jacobs, T., Junge, T. and Pastewka, L. (2017). Quantitative characterization of surface topography using spectral analysis. 5 (1).

[51]. Jain, R. and Pitchumani, R. (2017). Fractal Model for Wettability of Rough Surfaces. American Chemical Society Publications, Langmuir. 33: 7181-7190.

[52]. Mitra, S., Kumar Gunda, N.S. and Mitra, S.K. (2017). Wetting characteristics of underwater micro-patterned surfaces. RSC Adv. 7: 9064-9072.

[53]. Jain, R. (2017). Investigations on Multiscale Fractal-textured Superhydrophobic and Solar Selective coatings. MS Thesis. Faculty of the Virginia Polytechnic Institute and State University.

[54]. Kulatilake, P.H.S.W. and Um, J. (1999). Requirements for accurate quantification of self-affine roughness using the variogram method. Int J Solids Struct. 35 (31): 4167-4189.

[55]. Chen, S.J., Zhu, W.C., Yu, Q.L. and Liu, X.G. (2016). Characterization of anisotropy of joint surface roughness and aperture by variogram approach based on digital image processing technique. Rock Mech Rock Eng. 49 (3): 855-876.

[56]. Li, Y. and Huang, R. (2015). Relationship between joint roughness coefficient and fractal dimension of rock fracture surfaces. International Journal of Rock Mechanics & Mining Sciences. 75: 15-22.

[57]. Perfect, E. (2005). Modeling the primary drainage curve of prefractal porous media. Vadose Zone Journal. 4 (4): 959-966.

[58]. Rasouli, V. and Tokhmechi, B. (2010). Difficulties in Using Geostatistical Models in Reservoir Simulation. SPE 126191. Egypt.

[59]. Ojha, S.P, Misra, S., Sinha, A., Dang, S., Sondergeld, C. and Rai, C. (2017). Estimation of Pore Network Characteristics and Saturation-Dependent Relative Permeability in Organic-Rich Shale Samples Obtained from Bakken. WolfCamp, and Woodford Shale Formations, SPWLA 58th Annual Logging Symposium. pp. 17–21.

[60]. Suleimanov, A.B., Guseynova, N.I. and Veliyev, E.F. (2017). Control of Displacement Front Uniformity by Fractal Dimentions, SPE-187784-MS.

[61]. Malinverno, A. (1990). A Simple Method to Estimate the Fractal Dimension of Self-Affine Series. Geophysical Research Letters. 17 (11): 1953-1956.

[62]. Rahman, Z., Slob, S. and Hack, R. (2006). Deriving roughness characteristics of rock mass discontinuities from terrestrial laser scan data. IAEG, The Geological Society of London, No. 437.

[63]. Arizabalo, R.D., Oleschko, K., Korvin, G., Ronquillo, G. and Cedillo-Pardo, E. (2004). Fractal and cumulative trace analysis of wire-line logs from a well in a naturally fractured limestone reservoir in the Gulf of Mexico. Geofísica Internacional. 43 (3): 467-476.

[64]. Xie, H.P. and Pariseau, W.G. (1994). Fractal estimation of rock joint roughness coefficient, Sci. China. 24 (5): 524-530.

[65]. Askari, M. and Ahmadi, M. (2007). Failure process after peak strength of artificial joints by fractal dimension. Geotech Geol Eng. 25 (6): 631-637.

[66]. Maerz, N.H., Franklin, J.A. and Bennett, C.P. (1990). Joint roughness measurement using shadow profilometry. Int. J. Rock Mech. Min. Sci. Geomech. Abstr. (27): 329-343.

[67]. Bae, D., Kim, K., Koh, Y. and Kim, J. (2011). Characterization of joint roughness in granite by applying the scan circle technique to images from a borehole televiewer. Rock Mech. Rock Eng. 44: 497-504.

[68]. Xu, H.F., Zhao, P.S., Li, C.F. and Tong, Q. (2012). Predicting joint roughness coefficients using fractal dimension of rock joint profiles. Appl. Mech. Mater. 170-173: 443-448.

[69]. Tideman, T.N. (1987). Independence of Clones as a Criterion for Voting Rules, Social Choice and Welfare, Springer-Verlag. 4: 185-206.

[70]. Young, H.P. and Levenglick, A. (1978). A Consistent Extension of Condorcet's Election Principle. SlAM Journal on Applied Mathematics. 35: 285-300.

[71]. Newenhizen, J.V. (1992). The Borda Method is most likely to Respect the Condorcet Principle. Econ. Theory. 2: 69-83.

[72]. Moulin, H. (1988). Axioms of co-operative decision making. Econometric Society Monographs. Cambridge University Press. Cambridge.

[73]. Fishburn, P.C. (1984). Discrete Mathematics in Voting and Group Choice. 5 (2): 263-275.

[74]. Saari, D. (2000). Chaotic Elections! A Mathematician Looks at Voting. Providence, R.I., American Mathematical Society.

[75]. Vetter, W. (1970). Derivative operations on matrices. IEEE Trans. Autom. Control. 15: 241-244.

[76]. Rafek, A.G., Hussin, A., Lai Goh, T. and Serasa, A.S. (2017). Peak Friction Angle Estimation from Joint Roughness Coefficient of Discontinuities of Limestone in Peninsular Malaysia, Sains Malaysiana. 46 (2): 181-188.

اصلاح رتبه‌بندی ضرایب زبری درزه بارتون با رویکرد ترکیب اطلاعات مبتنی بر روش‌های فرکتالی و تبدیل موجک

محمد لطفی و بهزاد تخم‌چی*

دانشکده مهندسی معدن، نفت و ژئوفیزیک، دانشگاه صنعتی شاهرود، ایران

ارسال ۲۰۱۸/۱۰/۲۴، پذیرش ۲۰۱۹/۶/۱

* نویسنده مسئول مکاتبات: tokhmechi@ut.ac.ir

چکیده:

زبری شکستگی‌ها پارامتر چالش‌برانگیز و مهمی است که در انواع مطالعات و با رویکردهای گوناگون مورد بررسی قرار می‌گیرد. در این میان، ضرایب زبری درزه بارتون (JRC)، شاخص کاملاً شناخته شده‌ای است که به صورت گسترده در این مطالعات به عنوان مبنا به کار می‌رود. در این پژوهش، با استفاده از روش‌های مبتنی بر هندسه فرکتال و تبدیل موجک، زبری هر یک از پروفیل‌های JRC اندازه‌گیری و بُعد آن‌ها محاسبه شد. برخلاف انتظار منطقی در خصوص لزوم وجود روند افزایشی در نتایج به دست آمده، این روند در خروجی روش‌ها دیده نمی‌شود. در حالی که چنین رخدادی، فارغ از مقادیر زبری بوده و تصمیم‌گیری با استفاده از این شاخص را با ابهام جدی همراه می‌کند. در واقع برای شاخص مبنا، رتبه‌بندی‌های متفاوتی از هر یک روش‌ها که هرکدام برآمده از تئوری‌های متقنی هستند مشاهده می‌شود و این موضوع محل مناقشه خواهد بود. برای حل این مسئله و دریافت پاسخی پایدار، دو روش ترکیب اطلاعاتی کندورسه و شمارش بوردا مورد استفاده قرار گرفت. در ترکیب نتایج و رتبه‌بندی جدید با استفاده از روش کندورسه، شرایط مبهمی در مورد سه پروفیل ۴، ۵ و ۶ مشاهده می‌شود. این ابهام شامل برابری تعداد برنده‌ها، بازنده‌ها و برابری‌های رخ داده در ماتریس جفتی مقایسه‌ای است. برای حل این عدم‌قطعیت، روش شمارش بوردا مورد استفاده قرار گرفت. با رفع مشکل رخ داده و اصلاح پروفیل‌ها از طریق رتبه‌بندی مجدد ضمن ارائه یک رویکرد جدید، شاخص جدیدی تحت عنوان JRCN ارائه شده است. محاسبه مجموع مربعات خطا برای منحنی‌های JRC و JRCN نشان می‌دهد که مقدار خطا در شاخص جدید ارائه شده (JRCN)، کاهش و بهبود یافته است. علاوه بر این در شاخص جدید از نتایج تمامی روش‌های مبتنی بر تئوری‌هایی با منطق پذیرفته شده استفاده شده است؛ بنابراین می‌توان برای بررسی زبری از شاخص JRCN به عنوان جایگزین JRC استفاده نمود تا ضمن به‌کارگیری از یک استاندارد واحد، به پاسخی پایدار دست یافت.

کلمات کلیدی: ناهمواری، بُعد، تصمیم‌گیری، ترکیب اطلاعات، عدم قطعیت.